ORIGINAL ARTICLE

High electrochemical performance of high-voltage $LiNi_{0.5}Mn_{1.5}O_4$ by decoupling the Ni/Mn disordering from the presence of Mn^{3+} ions

Junghwa Lee, Chaeah Kim and Byoungwoo Kang

Electrochemical activity in high-voltage spinel $LiNi_{0.5}Mn_{1.5}O_4$ (LNMO) is strongly affected by the disordering of Ni/Mn and the presence of Mn^{3+} ions. However, understanding the effect of the Ni/Mn disordering or the presence of Mn^{3+} ions on electrochemical properties is not trivial because disordering is typically coupled with the presence of Mn^{3+} ions. Here, we demonstrate for the first time that the doping of Li instead of Ni increases Ni/Mn disordering, which is decoupled from the presence of Mn^{3+} ions. The resultant material has a particle size of ~ 1–2 µm and can achieve 120 mAh g^{-1} at 10 C for 50 cycles and further deliver about 60 mAh g^{-1} even at a rate of ~ 60 C (1 min discharge). Superior electrochemical performance is achieved by increased solid-solution phase transition behavior, which is caused by increased Ni/Mn disordering during delithiation. By decoupling, we find that the electrochemical properties in LNMO strongly depend on the phase transformation behavior and that the Ni/Mn disordering, rather than Mn^{3+} ions, affects the phase transformation by increasing the solid-solution reaction. The fundamental understanding gained from this work could be applied to the development of other phase-separating compounds to improve their electrochemical performance.

INTRODUCTION

For a lithium-ion battery, a high energy density is an essential requirement for novel applications such as plug-in hybrid electric vehicles and electric vehicles. Increasing the redox potential of cathode materials is an effective way to achieve high energy density in the cell. For this purpose, high-voltage spinel $LiNi_{0.5}Mn_{1.5}O_4$ is a promising cathode material for LIBs[1–3] because it has a high redox potential of about 4.7 V, which makes its energy density (650 W h kg^{-1}) 20% higher than that of the conventional $LiCoO_2$. However, the electrochemical properties of LNMO spinel depend on several factors, such as its structure,[3,4] the quantity of Mn^{3+} ions,[5,6] the particle size[2,7] and the morphology of particles.[8] Among these factors, the structure of the spinel has a critical influence on its electrochemical performance.[9–11] The LNMO structure is dictated by the ordering of Ni and Mn at two octahedral sites, which results in two spinel forms: disordered and ordered. The Ni and Mn in the ordered spinel are well ordered in two distinct octahedral sites, 4b sites for Ni and 12d sites for Mn, whereas the Ni and Mn in the disordered spinel are randomly distributed in 16d octahedral sites.[1,12] In the ordered spinel, the ordering of Ni/Mn exists without Mn^{3+} ions because a second annealing process at < 700 °C simultaneously leads to the ordering of Ni/Mn on two distinct octahedral sites and the oxidation of Mn^{3+} ions into Mn^{4+} ions. However, the disordered spinel shows both the disordering of Ni/Mn and the presence of Mn^{3+} ions. The correlation

of the disordering of Ni/Mn with the quantity of Mn^{3+} ions is due to the synthesis conditions, such as the heating temperature, cooling speed and post-annealing.[9] Typically, disordering of Ni/Mn can be induced by controlling the quantity of Mn^{3+} ions that originate from the loss of oxygen at a temperature process > 700 °C or quenching processes.[13,14] The decoupling of Ni/Mn disordering from the presence of Mn^{3+} ions in the disordered spinel has not yet been reported. As a consequence, electrochemical properties of the disordered spinel strongly depend on both the disordering of Ni/Mn and the presence of Mn^{3+} ions.

The Mn^{3+} ions in the disordered spinel improve the electrochemical performance because they can increase the electronic conductivity to approximately two orders of magnitude higher than that of the ordered spinel.[7,9,15] However, the presence of Mn^{3+} ions can negatively affect the electrochemical properties of the LNMO spinel because Mn^{3+} ions easily transform into Mn^{2+} ions through a disproportion reaction, and the Mn^{2+} ions then easily dissolve into the electrolyte, especially at high operating potential and an elevated temperature. As a result, the presence of Mn^{3+} ions can shorten the cycling and storage life of a cell even though the electronic conductivity of the disordered spinel is increased.[16]

The disordering of Ni/Mn in the disordered spinel also strongly affects the electrochemical performance because the disordering of Ni/Mn affects the phase transformation behavior by extending the

Department of Materials Science and Engineering, Pohang University of Science and Technology (POSTECH), Pohang, Korea
Correspondence: Professor B Kang, Department of Materials Science and Engineering, Pohang University of Science and Technology (POSTECH), 77 Cheongam-Ro, Nam-Gu, Pohang 790-784, Korea.
E-mail: bwkang@postech.ac.kr

solid-solution reaction for extracting lithium.[1,17,18] Considering that two distinct two-phase reactions occur during charging, the increase of the solid-solution reaction in the disordered spinel can substantially improve the electrochemical properties by reducing the mechanical stress/strain due to lattice mismatches in the phases.[4] As a result, many efforts have focused on increasing the amount of Ni/Mn disordering in the LNMO spinel. The main strategy to increase Ni/Mn disordering is by controlling Mn^{3+} ion contents in the sample. The disordering of Ni/Mn in the LNMO spinel increases as the quantity of Mn^{3+} ions increases by controlling the experimental conditions. For example, a large amount of Ni/Mn disordering can be introduced by a quenching process via a large reduction of Mn^{4+} ions, and this enhances the Li^+ ion transport, resulting in excellent electrochemical properties.[13] However, controlling the cooling rate in the LNMO spinel easily introduces nickel-rich rock salt phases, such as $Li_{1-x}Ni_xO$ or $Ni_{1-x}O$, which can negatively affect the electrochemical properties.[14] The other approach to increase Ni/Mn disordering is the doping of metals instead of Ni because the charge compensation can be satisfied by the increase of Mn^{3+} ions, which affect the disordering of Ni/Mn.[5,15,19–21] The doping of Cr^{3+} ions instead of Ni substantially increases the Ni/Mn disordering because they increase the Mn^{3+} ion content in the spinel. A Cr-doped LNMO spinel can achieve enhanced electrochemical properties.[5] Therefore, a disordered LNMO spinel can achieve better electrochemical performance than an ordered spinel because it has an extended solid-solution reaction during charging/discharging, leading to facile phase transformation[1,13,17] and high electronic conductivity originating from the Mn^{3+} ions.[7,9] However, the origin of the enhanced electrochemical properties in the disordered spinel is not clear because of the coupling of the Ni/Mn disordering with the Mn^{3+} ions. Understanding this origin is essential for optimizing the electrochemical properties of LNMO. Recent calculations have shown that the solid-solution phase transformation in the spinel results from the disordering of Ni/Mn, not from Mn^{3+} ions.[10,11] However, there are no experimental data supporting this calculation because controlling the Ni/Mn disordering to optimize electrochemical performance without the presence of Mn^{3+} ions has not been feasible. As a result, understanding the effect of disordering or the effect of Mn^{3+} ions on electrochemical properties is experimentally very important because the decoupling of the Ni/Mn disordering from the Mn^{3+} ions can help in optimizing the electrochemical performance of the LNMO spinel.

In this study, we doped the spinel with Li instead of Ni to demonstrate that the Ni/Mn disordering can be decoupled from the presence of Mn^{3+} ions. The Li doping combined with a long additional annealing at 700 °C increased the disordering of Ni/Mn in the spinel but minimized the quantity of Mn^{3+} ions. This allowed us to determine that controlling the amount of Ni/Mn disordering in the spinel is a more important factor for achieving superior electrochemical performance than is the presence Mn^{3+} ions. Using this material, we revealed that the disordering of Ni/Mn strongly affects the phase transformation, leading to the increase of the solid-solution reaction in delithiation, as predicted in calculations, and that the increased solid-solution reaction leads to superior electrochemical performance.

MATERIALS AND METHODS
Material synthesis
$LiNi_{0.5}Mn_{1.5}O_4$ was synthesized by solid-state reaction.[2] Appropriate ratios of Li_2CO_3, MnO_2 and $NiCO_3$ were ball-milled in acetone at 12 h. Li-doped samples had a Li:Ni:Mn ratio of 1.1:0.45:1.5. Dried mixture powders were

pelletized and then calcined at 900 °C for 12 h in air. After calcination, the pellets were ground, re-pelletized, and then annealed at 700 °C for 48 h in air.

Material characterizations
X-ray diffraction (D/MAX-2500/PC) measurement using Cu Kα ($\lambda = 1.54$ Å) radiation was used to identify the crystalline phase of the synthesized powders from 10 to 80° at a rate of 0.05° per second. The lattice parameter of each sample and the quantity of impurities were determined using X'Pert Highscore Plus software (PANalytical B. V., Almelo, The Netherlands). Particle size and morphology were observed using a field emission scanning electron microscope (FE-SEM, FEI/Philips, XL30S-FEG). The powders were coated with platinum via evaporation for SEM measurement.

Electrochemical measurements
For the galvanostatic electrochemical test, the lithium metal half cells were assembled using a Swagelok cell. The composite electrode weight ratio of (Active material 80 wt% : super-P (carbon black, Timcal) 5 wt% : carbon nano-fiber 10 wt% : binder 5 wt% (PVDF)) was prepared by spreading a slurry mixture on Al foil. The active material loading was 2–4 mg cm^{-2}. The active cathode and a lithium metal anode were separated by a porous polypropylene film (Celgard 2400, Celgard Inc, Charlotte, NC, USA). The electrolyte used was 1 M $LiPF_6$ dissolved in an EC/DEC (1:1) solution. The cell was operated over a range of 3.0–5.0 V vs Li/Li^+ at room temperature.

RESULTS AND DISCUSSION
Effect of Li doping on structure: increase of Ni/Mn disordering in the ordered spinel framework
Synthesized $LiNi_{0.5}Mn_{1.5}O_4$ (bare LNMO) and $Li_{1.1}Ni_{0.45}Mn_{1.5}O_4$ (Li-doped sample) showed similar X-ray diffraction patterns (Figure 1a) after a second annealing at 700 °C for 48 h. The samples also had similar lattice parameters: 8.166 Å for the bare sample and 8.168 Å for the Li-doped sample (Supplementary Table S1). The lattice parameters for both the samples were quite close to that of the ordered spinel, with a $P4_332$ space group.[1] Neither sample had any rock salt-related phase, such as NiO or Li_xNi_yO, but the Li-doped sample had a trace of the Li_2MnO_3 phase (Figure 1a, asterisks). Both samples showed additional peaks at ~35 and 40° (Figure 1a), but these were much weaker in the Li-doped sample than in the bare sample. These additional peaks originate from the ordering of Ni and Mn in two octahedral sites; therefore, the two samples had different degrees of Ni/Mn ordering. The weakening of these peaks in the Li-doped sample indicates that its cations are less ordered than those in the bare sample. Raman spectra (Supplementary Figure S2) further confirmed that the Li-doped sample has a large amount of Ni/Mn disordering, indicated by broad peaks at ca. 400, 490 and 630 cm^{-1} that become increasingly intense as Ni/Mn ordering increases.[22] Hence, a Li-doped sample can have a larger disordering of Ni/Mn than the bare sample even with the second annealing at 700 °C for 48 h.[1] The two samples had similar particle size (1–2 μm) and morphology (Figures 1b and c).

The increase of Ni/Mn disordering in the Li-doped sample was also confirmed by the voltage gap between the Ni^{2+}/Ni^{3+} and Ni^{3+}/Ni^{4+} redox potentials,[10] which was ~35 mV in the Li-doped sample and ~21 mV in the bare sample (Supplementary Figure S3). Because the voltage gap increases with the disordering of Ni/Mn in the LNMO spinel structure,[4,20] the observed difference in the voltage gap indicates that Ni/Mn disordering was greater in the Li-doped sample than in the bare sample even though the two samples were annealed under the same conditions.
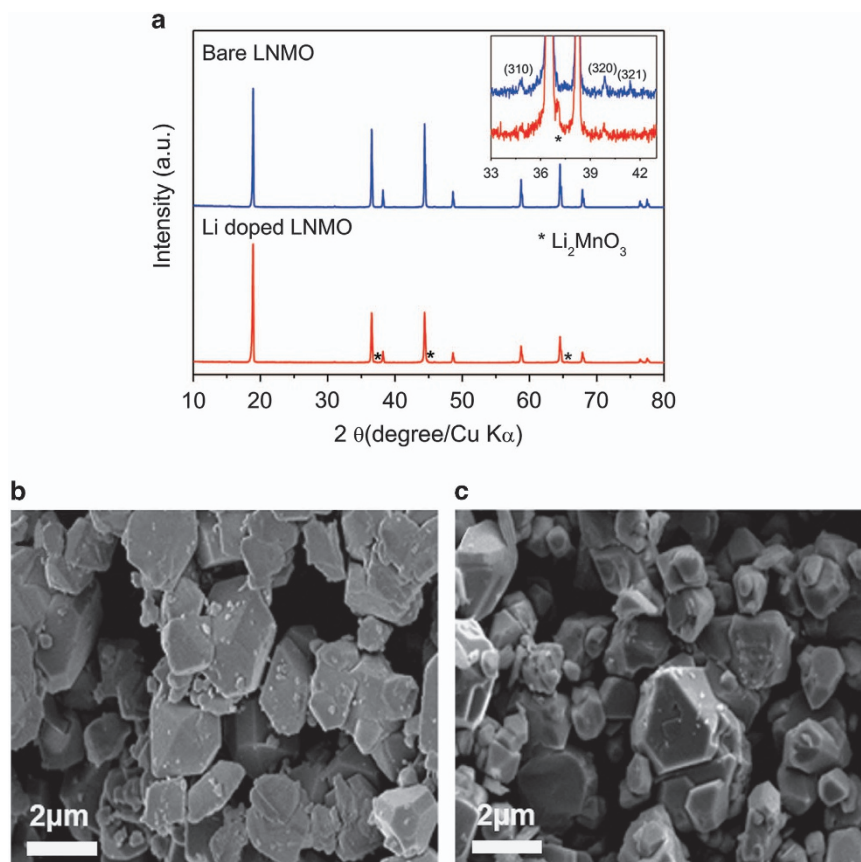
Figure 1 X-ray diffraction patterns of (**a**) bare $LiNi_{0.5}Mn_{1.5}O_4$ (LNMO) and Li-doped LNMO and comparison of the superstructure peak at (310), (320) and (321) plane in both sample asterisk: signal of Li_2MnO_3. Scanning electron microscope (SEM) image of (**b**) the bare LNMO and (**c**) the Li-doped LNMO.

Absence of Mn^{3+} ions in the Li-doped sample: the Li-doped sample has almost all Mn^{4+} ions

To investigate the presence of Mn^{3+} ions in the Li-doped sample and the bare sample, the two samples were electrochemically evaluated with a disordered LNMO with both Ni/Mn disordering and Mn^{3+} ions as a reference sample (Figure 2). The three samples showed different voltage plateau behavior at ~4 V; this difference originates from the redox reaction of the Mn^{3+}/Mn^{4+} couple. Therefore, the length of the voltage plateau at ~4 V indicates the relative quantity of Mn^{3+} ions in the samples.[5] To compare this amount in the three samples, the ratios of the capacity of 3.80 and 4.25 V to the total discharge capacity were calculated (Figure 2b).[5] In the bare sample and the Li-doped sample, the contribution of Mn^{3+} ions to the total discharge capacity was only 2–3%, which indicates that the quantity of Mn^{3+} ions is negligible in the two samples. However, in the disordered sample, 14% of the total capacity was caused by the redox reaction of the Mn^{3+}/Mn^{4+} couple, and this observation indicates that the quantity of Mn^{3+} ions in the disordered sample is large. These comparisons indicate that the re-annealing of the bare sample and the Li-doped sample substantially decreased the quantity of Mn^{3+} ions by oxidizing them to Mn^{4+}. The overall oxidation state of Mn in the Li-doped sample and the bare sample was almost 4+. Furthermore, X-ray Absorption Near-Edge Spectroscopy data (Supplementary Figure S4) confirmed that the bare and Li-doped samples contained Mn^{4+} ions almost exclusively. In the Li-doped sample, although Mn^{3+} ions were almost absent, this sample had greater Ni/Mn disordering than the bare sample, as shown by structural features (Figure 1). As a

consequence, the increase of Ni/Mn disordering in the Li-doped sample is not correlated with the presence of Mn^{3+} ions but may result from the doping of Li into the spinel.

The Li-doped sample showed greater Ni/Mn disordering than the bare sample even though the quantity of Mn^{3+} in the Li-doped sample was negligible. The Li doping of the spinel decoupled the presence of Mn^{3+} ions from the degree of the Ni/Mn disordering. Furthermore, the Li-doped sample showed lattice parameters similar to those of the ordered spinel. This indicates that the disordering of Ni/Mn in the spinel is not strongly correlated with the lattice parameters. Therefore, the lattice parameters in the disordered spinel with both the disordering and Mn^{3+} ions are good indicators for the quantity of Mn^{3+} ions, not the degree of Ni/Mn disordering. We have, for the first time, developed a simple procedure to decouple the disordering of Ni/Mn from the presence of Mn^{3+} ions. The results will help in understanding the effect of Ni/Mn disordering on the electrochemical properties of the LNMO spinel independently of the effect of Mn^{3+} ions.

Superior rate capability of the Li-doped sample than the bare sample due to the increase of Ni/Mn disordering in the Li-doped sample

The bare sample and the Li-doped sample showed quite different electrochemical properties at different discharge rates (Figure 3). The voltage curves of the bare sample and the Li-doped sample were measured at a 10 C discharge rate for 50 cycles (Figure 3a), and their capacity retention was measured (Figure 3b); in both cases, the
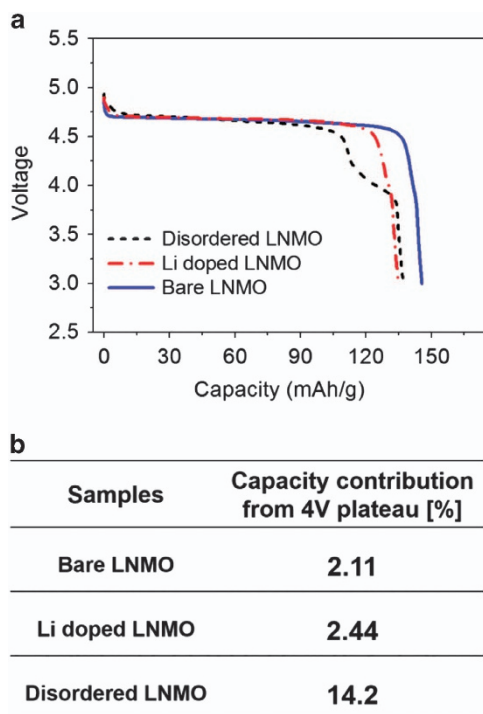
Figure 2 (**a**) Discharge voltage curve of the different samples at C/5 rate. The disordered sample (black), the Li-doped sample (red) and the bare sample (blue). (**b**) Summary of the ratio of the capacity from the 4 V plateau to the total capacity.

charging rate was C/5. A rate of n C corresponds to a full discharge in $1/n$ h. The bare sample at the rate of 10 C showed a large polarization, which led to substantial capacity fading from 110 to 85 mAh g^{-1} for 50 cycles. In contrast, the Li-doped sample at the rate of 10 C showed much lower polarization than the bare sample and retained the excellent capacity of ~ 120 mAh g^{-1} for 50 cycles even though the theoretical capacity in this sample is 134 mAh g^{-1}, which is lower than that in the bare sample due to the decrease in the quantity of Ni^{2+} ions in the Li-doped sample. Furthermore, the capacity retention of the Li-doped sample was as high as 86% of the theoretical capacity at 10 C, whereas the bare sample achieved 55% of the theoretical capacity at 10 C for 50 cycles (Figure 3b).

The Li-doped sample achieved superior electrochemical performance, especially the very high rate capability compared with that of the bare sample. The bare sample did not show any measurable capacity at discharge rates > 30 C, whereas the Li-doped sample showed superior rate capability (Figures 3c and d). At a discharge rate of 38 C, the Li-doped sample achieved a capacity of 120 mAh g^{-1}, which is 89% of the theoretical capacity. At the rate of 48 C, it delivered 90 mAh g^{-1}, and even at a rate of 58 C (~1 min), it achieved 60 mAh g^{-1}, which is 44% of the theoretical capacity. This very high rate capability indicates that the Li-doped sample has much better kinetics than the bare sample. It also implies that the Mn^{3+} ions in the spinel are not necessary for achieving superior rate capability.

Furthermore, both samples had similar physical properties, such as average particle size (1–2 μm), and faceted morphology (Figure 1); therefore, the superior electrochemical performance of the Li-doped sample cannot be a result of particle size or morphology. The main differences between the bare sample and the Li-doped sample are the degree of Ni/Mn disordering and the presence of Li$_2$MnO$_3$ in the Li-doped sample. The existence of an Li$_2$MnO$_3$ impurity phase cannot

strongly affect the electrochemical properties of the Li-doped sample because of the poor electrochemical activity of Li$_2$MnO$_3$, especially at high rates.[23] Therefore, the superior electrochemical performance appears to be related to the increase of Ni/Mn disordering in the Li-doped sample; that is, the electrochemical property of the spinel is strongly affected by the disordering of Ni/Mn and not by the presence of Mn^{3+} ions.

The disordering of Ni/Mn in the Li-doped sample changes the phase transition mechanism and leads to increases in the solid-solution phase transformation behavior during charging

To investigate the effect of Ni/Mn disordering on the electrochemical properties, especially the phase transformation behavior, *ex situ* X-ray diffraction patterns of the bare sample and the Li-doped sample were measured at different states of charge during charging (Figure 4).

During delithiation, both samples showed three cubic phases: LiNi$_{0.5}$Mn$_{1.5}$O$_4$ (LNMO), Li$_{0.5}$Ni$_{0.5}$Mn$_{1.5}$O$_4$ (L$_{0.5}$NMO) and Ni$_{0.5}$Mn$_{1.5}$O$_4$ (NMO) (Figure 4). However, the appearance and existence of the three phases differed between the two samples. In the bare sample (Figure 4a), the LNMO phase existed in a wide range of compositions for ~$0.25 \leqslant x \leqslant 1.0$ (x in Li$_x$NMO); the L$_{0.5}$NMO started to appear at $x = 0.75$ and existed in a wide range of compositions for ~$0.1 \leqslant x \leqslant 0.75$. After further delithiation, NMO started to appear for $0.25 \leqslant x \leqslant 0.5$ and existed until the end of the charge. In the bare sample, a delayed phase transformation from LNMO to Li$_{0.5}$NMO occurred at the beginning of the charge because L$_{0.5}$NMO started to appear at $x = 0.75$, not just after delithiation. This delayed phase transformation indicates that LNMO initially has a certain composition range of solid-solution reaction regions. However, in the bare sample, the range of the solid-solution reaction of the LNMO was limited when $x \leqslant 0.75$. Furthermore, in the bare sample, the LNMO, L$_{0.5}$NMO and NMO phases coexisted at $x \sim 0.25$. The extended existence of the LNMO may cause the three phases to coexist, because that phase was observed up to $x = 0.25$. The three-phase coexistence indicates that the phase transformation in the bare sample can be inhomogeneous or incomplete, especially for the Li-rich phase, LNMO. From these results, it appears that the phase transformation of the bare sample goes through extended two-phase reactions with the coexistence of the three phases and a limited solid-solution region at the beginning of the charge. This result is similar to a previous observation.[4,20] The coexistence of the three phases with the two-phase reaction behavior can increase mechanical strains and stresses between phases and thereby cause poor rate capability.

In contrast, the Li-doped sample showed quite different phase transformation behavior (Figure 4b); in this sample, LNMO existed in a narrow range of composition from $x = 1$ to $0.25 \leqslant x \leqslant 0.5$ (x in Li$_x$NMO). However, L$_{0.5}$NMO did not appear until $x = 0.64$; this delay of the phase transformation from LNMO to L$_{0.5}$NMO indicates that the solid-solution reaction of LNMO increased compared with that of the bare sample. L$_{0.5}$NMO started to appear at $0.5 \leqslant x \leqslant 0.64$ and disappeared at ~$0.1 \leqslant x \leqslant 0.25$. Further delithiation led to the appearance of NMO at $x \sim 0.25$, and this phase existed until the end of the charge. NMO also showed a certain composition range of the solid-solution reaction at the end of charging. As a result, the two-phase reaction region was substantially limited in the Li-doped sample because the solid-solution reaction behavior increases in the LNMO and L$_{0.5}$NMO phases. The extended solid-solution reaction region in the Li-doped sample decreased mechanical stresses and strains between phases and improved the electrochemical performance, leading to superior rate capability.
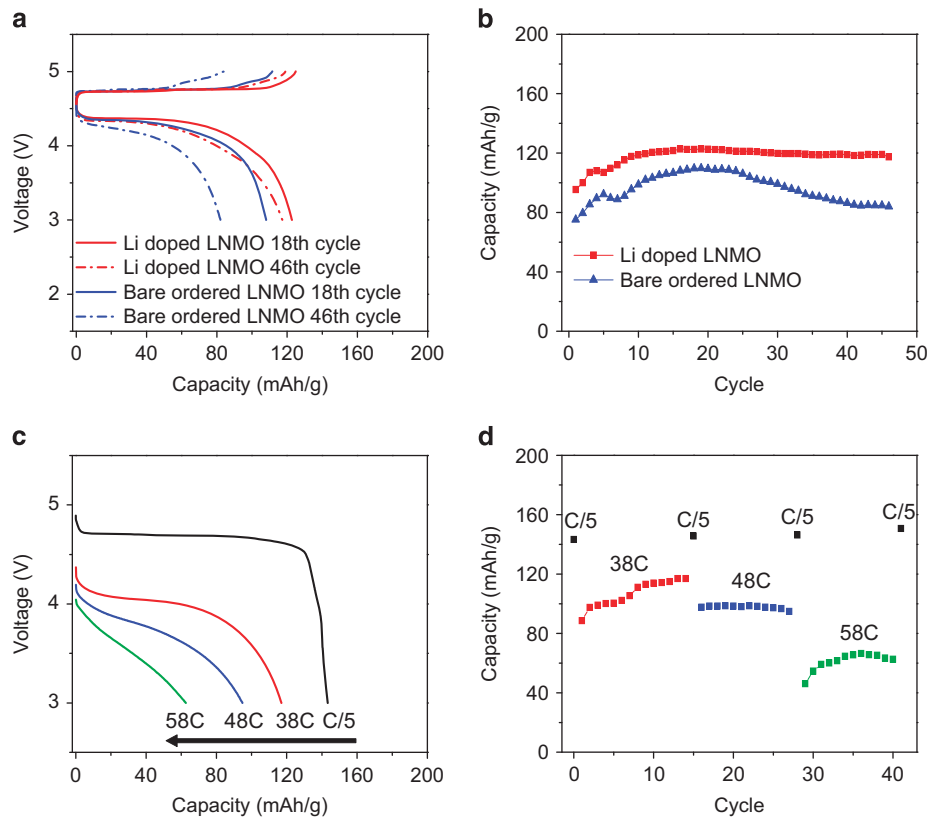
Figure 3 Electrochemical properties of the two samples. (**a**) The voltage curve of the bare sample and the Li-doped sample. (**b**) Capacity retention of both samples at discharge rate at 10 C. (**c**) Rate capability curve of Li-doped sample without the voltage hold at the end of charge. (**d**) Capacity retention of Li-doped sample. Charge rate was C/5 without holding the voltage and discharge rates were different. Cutoff voltages were set from 3 to 5 V.

The phase transformation behavior differed between the two samples (Figure 4c). The Li-doped sample showed extended solid-solution phase transformation behavior and a limited two-phase reaction region, whereas the bare sample showed limited solid-solution phase transformation behavior and an extended two-phase reaction with the coexistence of the three phases during charging.

The origin of different phase transformation behaviors in the two samples: different amounts of Ni/Mn disordering

The different phase transformation behaviors in the two samples during delithiation can have been caused by their different degrees of Ni/Mn disordering. The Li-doped sample showed a greater degree of Ni/Mn disordering than the bare sample. As a result, extended solid-solution behavior in the Li-doped sample can result from the large Ni/Mn disordering. This observation agrees very well with recent calculation results,[10,11] which indicate that a perfectly cation-ordered spinel with a space group of $P4_332$ resists the solid-solution phase transition behavior because the Ni/Mn ordering is incompatible with the ordering of Li$^+$ and vacancies during delithiation, whereas the introduction of Ni/Mn disordering into the spinel structure results in a gradual increase in stability for a solid-solution reaction, especially in a lithium-rich phase such as LNMO. The degree of Ni/Mn disordering strongly increases the solid-solution reaction during delithiation. The extended solid-solution reaction behavior significantly improves the electrochemical performance, thereby leading to superior rate capability. Considering that the Li-doped sample has a negligible quantity of Mn^{3+} ions, the Ni/Mn disordering, rather than the Mn^{3+}

ions, strongly affects the phase transformation behavior, leading to an increase in the solid-solution reaction.

Superior electrochemical performance of the Li-doped sample: increase of the solid-solution phase transition behavior

The Li-doped sample shows superior rate capability and capacity retention than the bare sample in Figure 3. This improved electrochemical performance of the Li-doped sample may result from the extended solid-solution reaction caused by the increase of cation disordering. In the LNMO spinel, phase transformation is a critical factor in achieving superior electrochemical performance because two distinct two-phase reactions with three cubic phases occur during delithiation and can induce large mechanical stresses and strains. Phase-separating compounds, such as LNMO, require additional energy for the formation of the secondary phase and the interface between two phases and accumulate significant coherency stress originating from the lattice misfit at the interface even though the compound is an isotropic polycrystalline material.[24]

Furthermore, the particle size strongly affects the phase transformation behavior because phase-separating reactions, such as the formation of a new secondary phase and interface, strongly depend on the particle size and lead to a large additional energy requirement. Therefore, a large particle size makes phase-separation behaviors difficult and thereby leads to poor electrochemical activity. Recently, Woodford *et al.*[25] reported that the critical particle size for coherency stress for spinel phases such as LiMn$_2$O$_4$ and LNMO is ~ 1 μm. This indicates that a particle size >1 μm can cause incoherent interfaces between the two phases and the formation of cracks or dislocations
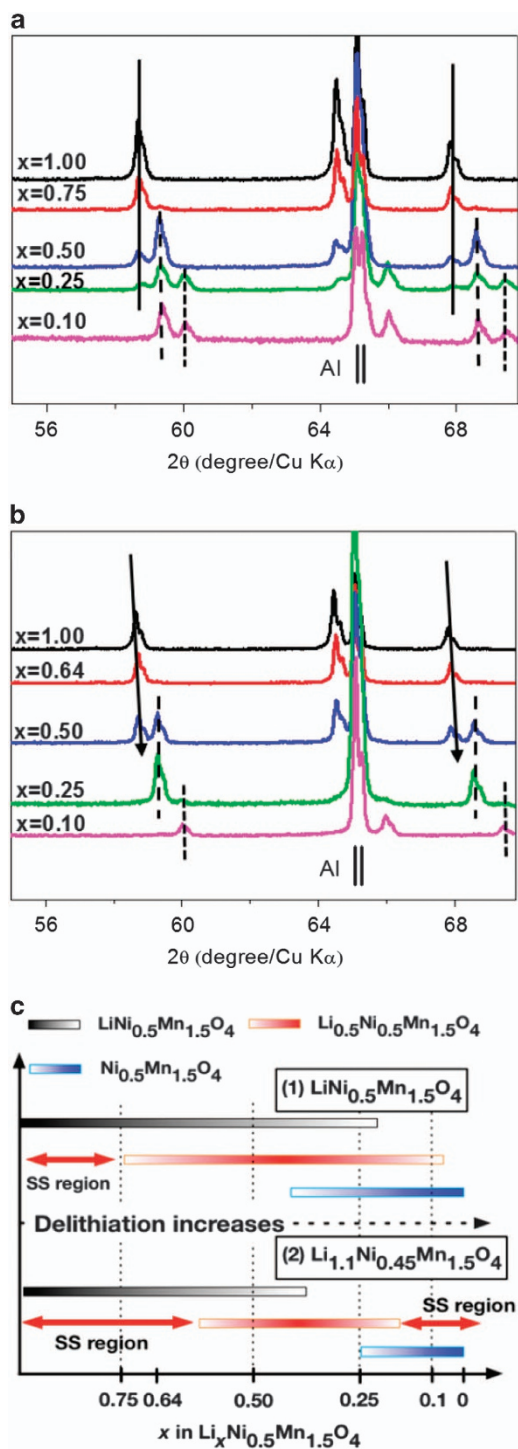
to poor kinetics of phase transformation and consequent poor electrochemical performance. Therefore, the phase transformation in the LNMO spinel is a critical factor for achieving superior rate capability because the LNMO spinel undergoes two distinct two-phase reactions with large particle size. However, the extended solid-solution reaction in the Li-doped sample strongly improves the electrochemical performance because its phase transformation involves neither large mechanical strain and stress nor additional formation energy. Furthermore, phase-separating behavior always leads to a flat voltage curve because of the first-order phase transformation. The flat voltage does not allow for homogeneous redox reactions in particles in the electrode.[26] The inhomogeneous redox reactions may cause incomplete transformation, leading to three-phase coexistence in the bare sample. However, the Ni/Mn disordering leads to a large voltage gap between the two redox reactions, which can help to facilitate complete phase transformation, thereby resulting in excellent electrochemical performance.

In summary, we present the first demonstration that Li-doping of LNMO decouples the Ni/Mn disordering from the presence of Mn^{3+} ions and substantially improves the electrochemical performance by increasing the solid-solution phase transition behavior during charging. The resulting material can achieve $120\,mAh\,g^{-1}$ at $10\,C$ for 50 cycles and can deliver $\sim 60\,mAh\,g^{-1}$ even at a rate of $\sim 60\,C$ (1 min discharging). By decoupling the Ni/Mn disordering from the presence of Mn^{3+} ions, we find that the phase transformation is the critical factor that influences the electrochemical performance of the high-potential LNMO spinel and that it is strongly affected by the disordering of Ni/Mn, which leads to the solid-solution reaction. These findings may be applied to develop other phase-separating compounds and to improve their electrochemical performance.

CONFLICT OF INTEREST

The authors declare no conflict of interest.

1 Ariyoshi, K., Iwakoshi, Y., Nakayama, N. & Ohzuku, T. Topotactic two-phase reactions of Li [$Ni_{1/2}Mn_{3/2}$]O_4 ($P4_332$) in nonaqueous lithium cells. *J. Electrochem. Soc.* **151**, A296–A303 (2004).

2 Ma, X., Kang, B. & Ceder, G. High rate micron-sized ordered $LiNi_{0.5}Mn_{1.5}O_4$. *J. Electrochem. Soc.* **157**, A925–A931 (2010).

3 Chemelewski, K. R. & Manthiram, A. Origin of site disorder and oxygen nonstoichiometry in $LiMn_{1.5}Ni_{0.5-x}M_xO_4$ (M = Cu and Zn) cathodes with divalent dopant ions. *J. Phys. Chem. C* **117**, 12465–12471 (2013).

4 Xiao, J., Yu, X., Zheng, J., Zhou, Y., Gao, F., Chen, X., Bai, J., Yang, X. Q. & Zhang, J. Interplay between two-phase and solid solution reactions in high voltage spinel cathode material for lithium ion batteries. *J. Power Sources* **242**, 736–741 (2013).

5 Xiao, J., Chen, X., Sushko, P. V., Sushko, M. L., Kovarik, L., Feng, J., Deng, Z., Zheng, J, Graff, G. L., Nie, Z., Choi, D., Liu, J., Zhang, J. G. & Whittingham, M. S. High-performance $LiNi_{0.5}Mn_{1.5}O_4$ spinel controlled by Mn^{3+} concentration and site disorder. *Adv. Mater.* **24**, 2109–2116 (2012).

6 Jafta, C. J., Mathe, M. K., Manyala, N., Roos, W. D. & Ozoemena, K. I. Microwave-assisted synthesis of high-voltage nanostructured $LiNi_{0.5}Mn_{1.5}O_4$ spinel: tuning the Mn^{3+} content and electrochemical performance. *ACS Appl. Mater. Interfaces* **5**, 7592–7598 (2013).

7 Kunduraci, M., Al-Sharab, J. F. & Amatucci, G. G. High-power nanostructured $LiMn_{2-x}Ni_xO_4$ high-voltage lithium-ion battery electrode materials: electrochemical impact of electronic conductivity and morphology. *Chem. Mater.* **18**, 3585–3592 (2006).

8 Zhou, L., Zhao, D. & Lou, X. D. $LiNi_{0.5}Mn_{1.5}O_4$ hollow structures as high-performance cathodes for lithium-ion batteries. *Angewandte Chemie.* **124**, 243–245 (2012).

9 Kim, J. -H., Huq, A., Chi, M., Pieczonka, N. P. W., Lee, E., Bridges, C. A., Tessema, M. M., Manthiram, A., Persson, K. A. & Powell, B. R. Integrated

Figure 4 *Ex situ* X-ray diffraction patterns of (**a**) bare sample $LiNi_{0.5}Mn_{1.5}O_4$ and (**b**) Li-doped sample $Li_{1.1}Ni_{0.45}Mn_{1.5}O_4$, $Li_xNi_{0.5}Mn_{1.5}O_4$ electrodes at different states of charge (SOC) (*x*). (**c**) Schematic diagram of the phase transformation at different SOCs for (1) the bare sample $LiNi_{0.5}Mn_{1.5}O_4$ and (2) the Li-doped sample $Li_{1.1}Ni_{0.45}Mn_{1.5}O_4$. SS, solid-solution reaction. Al peak represents the current collector.

that slow the phase transformation. Considering that the particle size of the two samples was $1–2\,\mu m$, which is larger than the critical particle size, the phase-separating reaction in the samples easily forms incoherent interfaces, which result in the formation of cracks that lead

nano-domains of disordered and ordered spinel phases in $LiNi_{0.5}Mn_{1.5}O_4$ for Li-Ion batteries. *Chem. Mater.* **26**, 4377–4386 (2014).

10 Lee, E. & Persson, K. A. Solid-solution Li intercalation as a function of cation order/disorder in the high-voltage $Li_xNi_{0.5}Mn_{1.5}O_4$ spinel. *Chem. Mater.* **25**, 2885–2889 (2013).

11 Lee, E. & Persson, K. A. Revealing the coupled cation interactions behind the electrochemical profile of $Li_xNi_{0.5}Mn_{1.5}O_4$. *Energy Environ. Sci.* **5**, 6047 (2012).

12 Cabana, J., Casas-Cabanas, M., Omenya, F. O., Chernova, N. A., Zeng, D., Whittingham, M. S. & Grey, C. P. Composition-structure relationships in the Li-ion battery electrode material $LiNi_{0.5}Mn_{1.5}O_4$. *Chem. Mater.* **24**, 2952–2964 (2012).

13 Zheng, J., Xiao, J., Yu, X., Kovarik, L., Gu, M., Omenya, F., Chen, X., Yang, X. Q., Liu, J., Graff, G. L., Whittingham, M. S. & Zhang, J. G. Enhanced Li^+ ion transport in $LiNi_{0.5}Mn_{1.5}O_4$ through control of site disorder. *Phys. Chem. Chem. Phys.* **14**, 13515–13521 (2012).

14 Liu, G., Park, K. -S., Song, J. & Goodenough, J. B. Influence of thermal history on the electrochemical properties of $Li[Ni_{0.5}Mn_{1.5}]O_4$. *J. Power Sources* **243**, 260–266 (2013).

15 Yi, T. -F., Xie, Y., Ye, M. -F., Jiang, L.-J., Zhu, R. -S. & Zhu, Y. -R. Recent developments in the doping of $LiNi_{0.5}Mn_{1.5}O_4$ cathode material for 5 V lithium-ion batteries. *Ionics* **17**, 383–389 (2011).

16 Gummow, R., De Kock, A. & Thackeray, M. Improved capacity retention in rechargeable 4 V lithium/lithium-manganese oxide (spinel) cells. *Solid State Ionics* **69**, 59–67 (1994).

17 Kim, J. H., Myung, S. T., Yoon, C. S., Kang, S. G. & Sun, Y. K. Comparative study of $LiNi_{0.5}Mn_{1.5}O_{4-\delta}$ and $LiNi_{0.5}Mn_{1.5}O_4$ cathodes having two crystallographic structures: $Fd\bar{3}m$ and $P4_332$. *Chem. Mater.* **16**, 906–914 (2004).

18 Kim, J. -H., Yoon, C., Myung, S. -T., Prakash, J. & Sun, Y. -K. Phase transitions in $Li_{1-\delta}Ni_{0.5}Mn_{1.5}O_4$ during cycling at 5 V. *Electrochem. Solid-State Lett.* **7**, A216–A220 (2004).

19 Shin, D. W., Bridges, C. A., Huq, A., Paranthaman, M. P. & Manthiram, A. Role of cation ordering and surface segregation in high-voltage spinel $LiMn_{1.5}Ni_{0.5-x}M_xO_4$ (M= Cr, Fe, and Ga) cathodes for lithium-ion batteries. *Chem. Mater.* **24**, 3720–3731 (2012).

20 Zhu, W., Liu, D., Trottier, J., Gagnon, C., Guerfi, A., Julien, C. M., Mauger, A. & Zaghib, K. Comparative studies of the phase evolution in M-doped $Li_xNi_{0.5}Mn_{1.5}O_4$ (M= Co, Al, Cu and Mg) by in-situ X-ray diffraction. *J. Power Sources* **264**, 290–298 (2014).

21 Zhong, G. B., Wang, Y. Y., Zhao, X. J., Wang, Q. S., Yu, Y. & Chen, C. H. Structural, electrochemical and thermal stability investigations on $LiNi_{0.5-x}Al_{2x}Mn_{1.5-x}O_4$ ($0 \leqslant 2x \leqslant 1.0$) as 5 V cathode materials. *J. Power Sources* **216**, 368–375 (2012).

22 Kunduraci, M. & Amatucci, G. Synthesis and characterization of nanostructured 4.7 V $Li_xMn_{1.5}Ni_{0.5}O_4$ spinels for high-power lithium-ion batteries. *J. Electrochem. Soc.* **153**, A1345–A1352 (2006).

23 Thackeray, M. M., Johnson, C. S., Vaughey, J. T., Li, N. & Hackney, S. A. Advances in manganese-oxide 'composite' electrodes for lithium-ion batteries. *J. Mater. Chem.* **15**, 2257–2267 (2005).

24 Woodford, W. H., Chiang, Y. -M. & Carter, W. C. Electrochemical shock in ion-intercalation materials with limited solid-solubility. *J. Electrochem. Soc.* **160**, A1286–A1292 (2013).

25 Woodford, W. H., Carter, W. C. & Chiang, Y. -M. Design criteria for electrochemical shock resistant battery electrodes. *Energy Environ. Sci.* **5**, 8014–8024 (2012).

26 Ouvrard, G., Zerrouki, M., Soudan, P., Lestriez, B., Masquelier, C., Morcrette, M., Hamelet, S., Belin, S., Flank, A. M. & Baudelet, F. Heterogeneous behaviour of the lithium battery composite electrode $LiFePO_4$. *J. Power Sources* **229**, 16–21 (2013).